Even Parity Rydberg States of Atomic Bismuth

A thesis submitted in partial fulfillment of the requirement
for the degree of Bachelor of Sciences with Honors in
Physics from the College of William and Mary in Virginia,

by

Kenneth L Baranowski

Accepted for _____Highest Honors_____
(Honors, High Honors, or Highest Honors)

_____
Dr. K. Grifioen Director

_____
Dr. W. E. Cooke Advisor

_____
Dr. W. J. Kossler

_____
Dr. I. Spitkovsky

Williamsburg, Virginia
May 2001

Table of Contents:

Even Parity Rydberg States of Atomic Bismuth

Honors Thesis by K. L. Baranowski

Abstract: Even parity photoionizing spectrum in atomic Bismuth is presented along with the associated quantum defects. These results are compared with other research on even parity Rydberg states. This work extends to higher *n* the $(6p^2\ ^3P_0)nd_{5/2}$ (n*=24.2,49.1), $(6p^2\ ^3P_0)nd_{5/2}$ (n*=24.8,34.8), and $6p^2\ ^3P_0\ ns_{1/2}$ (n*=25.2,36.3) series previously reported.

Introduction

Overview

Bismuth has a ground state configuration of $5d^{10}6s^26p^3\ ^4S^o_{3/2}$. This leaves the outermost p shell half empty with electrons, which have their spins aligned. Thus, the ground state is a system with only three active electrons in a $^4S^o_{3/2}$ configuration, which is isotropic with total angular momentum **J**=3/2. When one of the three $6p^3$ electrons is excited it occupies a state far removed from the remaining core electrons; this electron is termed a Rydberg electron. The remaining two electrons are designated core electrons although there are 80 other electrons tightly bound in a hard core. The core state with lowest energy for the two core electrons in the Bismuth ion is the $6p^2$ ($^3P_0$) state.

Zeeman, Back and Goudsmit[1] (1930) first investigated Bismuth's spectrum while investigating Zeeman splitting. Mrozowski[2] (1942) studied the arc spectrum of Bismuth using a cathode discharge tube. He photographed the emitted spectrum using a 30-foot spectrograph where he corrected 13 previous levels and recorded 28 new levels. Based on his analysis Moore[3] (1958) quoted an ionization potential of 58790 cm^{-1}. Joshi and

Srivastava[4] (1978) used the flash pyrolysis technique[5], with a 3 m vacuum spectrograph, to study higher energy states than previously reported. Using these single photon excitations, they then adjusted the ionization potential to 58765 cm^{-1}. Young, Mirza and Duley[6] (1980) studied Bismuth using three-photon hybrid resonances[i], where they adjusted the previous ionization potential to 58762.0 ± 0.3 cm^{-1}. George, Munsee and Vergés[7] (1985) used a Fourier-transform spectrometer[8] to study the single photon spectrum excited by a Raytheon C-director antenna. Using Iodine lines as a calibration, they deduced an ionization potential of 58760.0 ± 0.3 cm^{-1}. Later, this number was corrected to 58761.68 ± 0.1 cm^{-1} by Bühler[9] (1985), using two lasers (odd parity states) to n = 75. Mazzoni, *et al*[10] (1987) then studied the single photon spectrum of atomic Bismuth employing the flash pyrolysis technique [5] with a 3 m vacuum spectrograph. Mathews[11] (1989) used a King furnace[12] and a 6.6 m spectrograph. He gave the most recent ionization potential of 58761.65 ± 0.05 cm^{-1} using single-photon excitation to n = 63. Most recently, the spectrum of Bismuth has been studied by Yoo, Ruscic and Berkowitz[13] (1995) who studied the range between the $^3P_0$ series and the $^3P_2$ energies of Bi^+. In this study the authors reincarnated an older McPherson ultraviolet monochromater and a mass spectrometer to take their measurements. Therefore, besides the work by Young, Mirza and Duley [6] there have been no further studies of three-laser even parity photoionizing Bismuth. Furthermore, the laser line widths attained in this work are superior to the vuv spectrum, which has inherent pressure and Doppler shifts, which now determines the ionization potential. This work confirms the spectrum which Young, Mirza and Duley first found and probes the $ns_{1/2}$, $nd_{3/2}$ and $nd_{5/2}$ series to higher n* and with better resolution than has been previously reported.

[i] Referring to both molecular and atomic excitations

Bismuth

Rydberg studies of many other elements which have one valence electron have been reported in the literature (Li, Rb, Cs, Al[14], Ga, and In). Further research was done on two valence electron systems such as Sr[15], Ba, Sn and Pb[16,17]. Since Bismuth has three valence electrons this system is both classically and quantum-mechanically insoluble. Therefore, Bismuth is fundamentally more complicated, which explains the lack of a vast, well resolved spectrum.

The $6p^2$ ($^3P_0$) configuration is a p state, which is a superposition of two individual p states. But, this superimposed state's angular momentum and spin rapidly precesses around an axis at a rate of 5.2×10^{14} Hz. This creates a configuration that appears isotropic on long time scales, but which is anisotropic by its very nature. By learning how this core configuration interacts with Rydberg electrons we will learn how free electrons interact with anisotropic electron states including Bi^+. Using Rydberg electrons, we performed a precision scattering experiment by determining the energy levels of the $6p^2$ ($^3P_0$)ns$_{1/2}$, $6p^2$ ($^3P_0$)nd$_{3/2}$, and $6p^2$ ($^3P_0$)nd$_{5/2}$ series and noting the difference between these perturbed energy levels and the one electron like levels which have an isotropic core configuration with no structure.

Rydberg States

Rydberg electrons have a very high principle quantum number[ii]. Bismuth's $6p^2$ ($^3P_0$) core configuration is an anisotropic state in which the spin and angular momentum of the $^3P_0$ state precess around an axis. Since the Rydberg electron's radius from the nucleus: $r \propto n^2$, Rydberg electrons model the free electron-ion interaction and allow us to very precisely determine the strength of the interactions of the electrons as well as the anisotropy of the core $6p^2$ ($^3P_0$) configuration.

Rydberg electrons are far removed from the partially filled electronic states. A typical principle quantum number for a Rydberg electron is 20. A Rydberg electron is so far away from other electrons in the atom that it can be treated using the independent electron model. Here, the Rydberg electron experiences a coulombic potential dominated by the monopole term, and yet having higher order terms in the multipole expansion. Rydberg state analysis is a clever way of producing an easily maintained and reproducible collision experiment. Thinking classically, the electron does not have enough energy to escape the system and so it falls to the core, interacts with the core states according to the Coulomb force[iii] and then leaves the core until it repeats the cycle again, with a period of $2.4 \times 10^{-17} (n^*)^3$ seconds. So, the Rydberg electrons are individual, reproducible scattering experiments.

The Rydberg electron is loosely bound to the atom, so it is just below the ionization potential. If the Rydberg electron interacts quickly enough with the core electrons it will experience the anisotropic, (non-symmetric) potential of the $6p^2$ ($^3P_0$)

[ii] on the order of 20
[iii] $F=(Cq_1q_2)/(4\pi r^2)$

core state, which can perturb the Rydberg energy levels. This is the time dependent way of looking at the situation; however, there is also a time independent view.

The time independent view is called Configuration Interaction (CI). This view describes the core electrons as a linear superposition of two or more linearly independent configurations. In the case of Bismuth there are three series in which the core may be configured, however only the $^3P_0$ and $^3P_1$ have substantial mixing as can be seen in the Figure 1. An example is that we expect the $6p^2(^3P_0)nd\ ^2D_{3/2}$ series, but instead we have the $6p^2(^3P_0)nd\ ^2D_{3/2}$ plus either the $6p^2(^3P_1)\ nd\ ^2D_{5/2}$ or $6p^2(^3P_1)\ ns\ ^2S_{1/2}$, which are corrected by the quadrupole coupling. All of these are configurations have the same parity and total angular momentum **J**. The Rydberg electron is in a state that can only be described as a combination of several states. Both this time-independent view of the configuration mixing and the time dependent, configuration interaction, view will produce exactly the same results. In fact, one can create a rotating quadrupole by making a coherent superposition of the ^3P_J core states.

Figure 1: Configuration Interaction of $^3P_1$ and $^3P_0$ series in Bismuth, mixing occurs when electron is in a superposition of nearby energy states

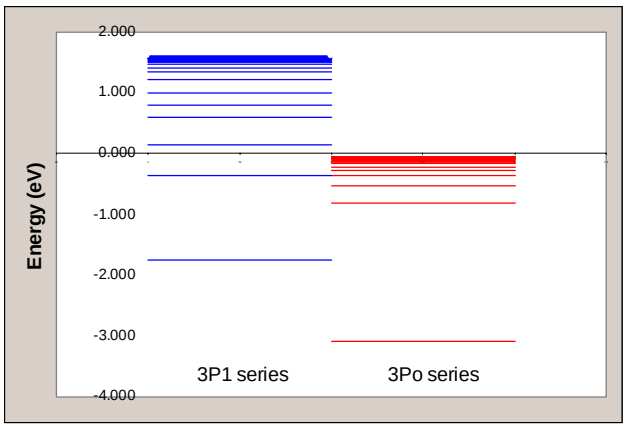

Energy levels for all bound electrons are discrete. Using Planck's law, $E=h\nu$, we recognize that in order to move an electron from one energy state to another the

electronic wave function absorbs energy (usually a photon). The new energy, E_{new}, will be: $E_{new} = E_{original} + E_{photon}$. The new Energy State will be populated for a time on the order of microseconds unless field ionization occurs or spontaneous emission causes the electron to decay to its original energy state. These energy states are perturbed hydrogenic energy states because the Rydberg electron primarily experiences incomplete shielding of the nucleus as it passes through the core electron. The deviation from the hydrogenic energy levels tells us about the strength of the interaction between the Rydberg electron and the core electrons. The Rydberg electron's energy, $E=-13.6/(n^*)^2$ eV, where $n^* = n-\delta$ for a quantum defect δ. Most Rydberg series, if they are

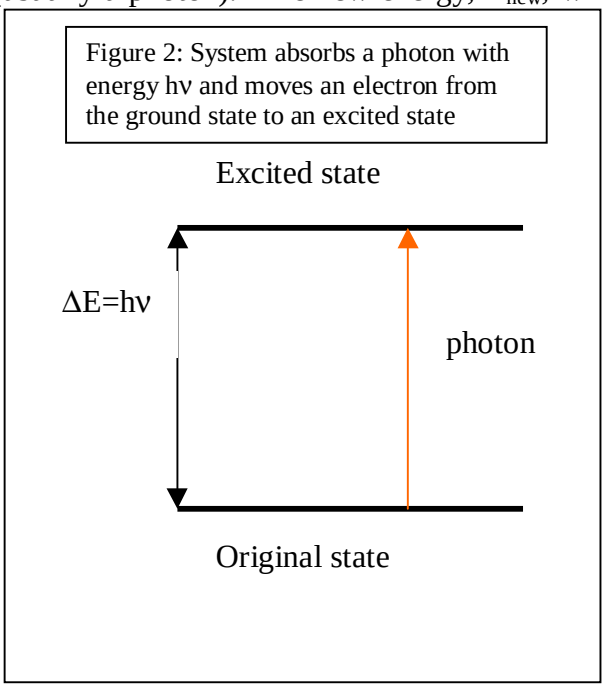

Figure 2: System absorbs a photon with energy hν and moves an electron from the ground state to an excited state

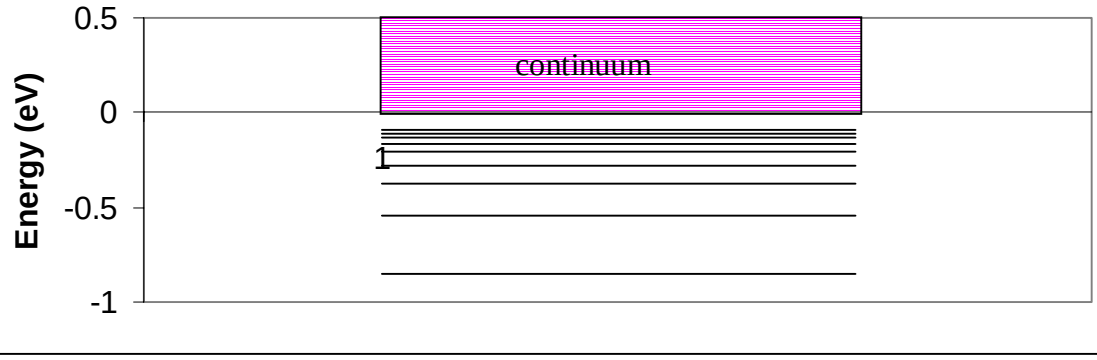

Figure 3: Energy states of Rydberg series, $E=-13.6/(n^*)^2$

not perturbed by configuration mixing, have a quantum defect δ that is nearly independent of n. This was measured by noting the relative movement of the energy levels to the ionization limit as n changed. Lasers, which are very narrow banded (~0.3 cm^{-1}), populate the Rydberg states and are explained in detail in the Experimental Apparatus section including exactly which resonance and virtual states were used.

Experimental Apparatus

Atomic Beam

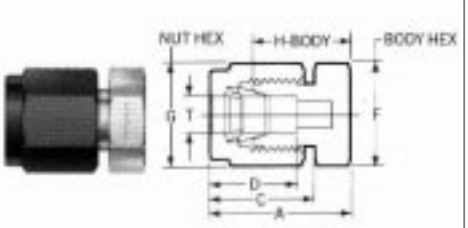

Figure 4: 1st oven system, stainless steel plug and cap system, solid Bi is loaded into the H-Body section

The atomic beam necessary for Rydberg research can be produced in a variety of different ways. The first apparatus used in this work was the "cannon" apparatus, with the oven seen in Figure 4. The commercial Bismuth used in this experiment was 99% pure Bismuth in solid form and acquired from Alfa Aesar. The Bismuth had been molded into needles about 3 cm long and ½ cm wide. Ten grams of Bismuth, were loaded into the plug and cap system as can be seen in Figure 3. A hole, 1 mm in diameter, was drilled through the stainless steel plug into the main holding chamber so the Bismuth vapor would escape in only one direction. This oven with Bismuth was placed on a ceramic disk about 4 inches in diameter. On this disk sits a ceramic cylinder with wires that run through it. Outside this cylinder are a series of heat shields whose purpose is to concentrate the heat produced by the voltage running through the ceramic material into a small volume. The smaller the volume in which the heat is concentrated the greater the temperature of the stainless steel oven. Bismuth was selected, in part, for it's relatively low melting point. At 1021° C, Bismuth has a vapor pressure of 1 mm Hg[18]. There is a concern that Bismuth, with its half filled p shell, will bond with itself to produce Bi_2. Bowering[19] states that Bi and Bi_2 may be found, at 1000K, in equal abundances. Young, Mirza and Duley [6] actually studied atomic Bi by means of Bi_2 and did so by exciting the molecular bond with one laser and then breaking

the bond, which decayed into an excited state of atomic Bi, which could then be excited itself. However, since atomic Bi would be so easy to produce at temperatures, which are easily accessible, we proceed by heating the oven to 1021° C and producing a dense beam at 1 mm Hg of atomic Bi. However, after thoroughly cleaning and repairing the vacuum system on the "cannon chamber" the heater was continuing to malfunction. The cooling nozzle directly above the heater was removed and an eyepiece was installed. Something was wrong with this heater system, however high current did not heat the oven near 700° C, where the oven would have glowed bright orange. After being unable to correct this deficiency we decided that moving to the other chamber would be a good idea.

After the difficulties producing the atomic Bi beam in the cannon apparatus this apparatus was another option. Kathy-Anne Brickman had already used it this year in her research on the Rydberg states of Strontium[20]. The heating mechanism in this chamber is vastly different than that in the "cannon" chamber. In the second chamber the Bi needles were loaded into a hollow stainless steel tube. When the tube is loaded into the chamber heat shields similar to those in the "cannon" chamber surround it. One of these heat shields has a small 1 cm by 3 cm hole. It is thus imperative that the escaping Bi vapor exits the stainless steel tube through a hole that will direct the atomic beam through the hole

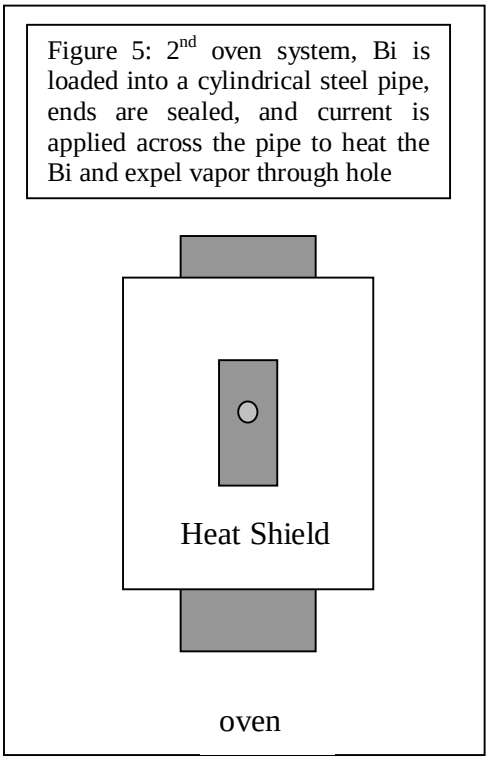

Figure 5: 2nd oven system, Bi is loaded into a cylindrical steel pipe, ends are sealed, and current is applied across the pipe to heat the Bi and expel vapor through hole

in the heat shield. This configuration can be seen in Figure 5.

After the placement of the hole in the cylinder is determined one of the ends of the tube is flattened. Next, Bi is loaded into the tube. Finally the other end of the tube is flattened, creating a space within the tube where the Bi cannot escape, except through the 1mm hole drilled into the side of the tube. Now that there is a space created for the Bi and a hole for the atomic Bi to escape we must heat the Bi to 1021° C to give an atomic beam with a density of 1 mm Hg. Passing a current through the stainless steel tube produces the heating.

Steel is a very poor conductor and thus will use the power[iv] supplied by a high current, low voltage, source to heat the stainless steel tube and also the Bi needles within the tube. This method does not always heat the material in the oven. The main concern with this type of oven is that since we are passing a current through steel, which is a poor conductor, it is possible that the material being studied will coat the interior of the oven and, if the material is a good conductor, will pass the current applied to the oven with little resistance and not heat the sample. Luckily, Bismuth is a poor conductor, explaining its use as a semiconductor, and so this effect will not cause problems in this work. The clear ratification of the heating of the oven is evident by viewing the oven through a window orthogonal to the incoming laser beams. Through this window the stainless steel oven glows orange at 700° C, also the hole that has been drilled in the tube can be viewed to verify that the oven has not clogged. We now have an atomic Bismuth beam, but in order to study Bismuth we need isolate Bismuth by removing the other

[iv] P=IV

constituents of the atmosphere in the chamber, we do this by using a well-engineered medium vacuum system.

After producing an atomic beam of Bismuth it is important to remove air particles to make sure the spectrum taken will be that of Bi and not that of Nitrogen or Oxygen. Both the cannon chamber apparatus and the other chamber employ the same two devices to attain medium vacuum levels. However, there are subtle differences between the apparatuses, which should be noted. Both systems use a fore pump to create a vacuum pressure down to $2x10^{-2}$ Torr. The fore pump uses chambers to trap gaseous molecules. Oil is used to seal these chambers until the pump expels the gaseous molecules through the exhaust line. The "cannon" chamber apparatus uses the tree setup seen in Figure 6 to connect the fore pump to the next vacuum pump, the diffusion pump.

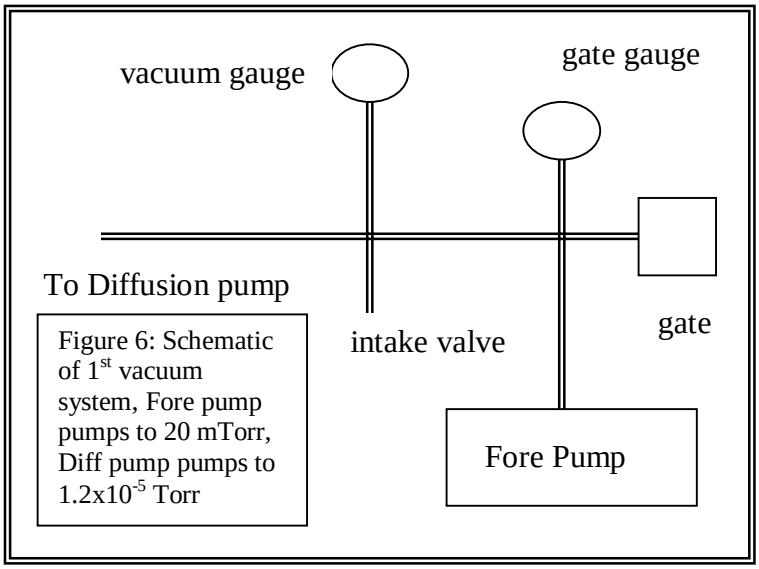

Figure 6: Schematic of 1st vacuum system, Fore pump pumps to 20 mTorr, Diff pump pumps to $1.2x10^{-5}$ Torr

A schematic of the diffusion pump can be seen in Figure 7. The diffusion pump uses synthetic oil to attain vacuum pressures of down to $1.2x10^{-5}$ Torr. Heating the synthetic oil and then passing the oil through a mechanism, which sprays the oil from the top of the diffusion pump chamber down to the base, produces this pressure. This spray captures gaseous particles to create a pressure gradient throughout the diffusion pump chamber. The fore pump then evacuates these captured particles from the diffusion pump

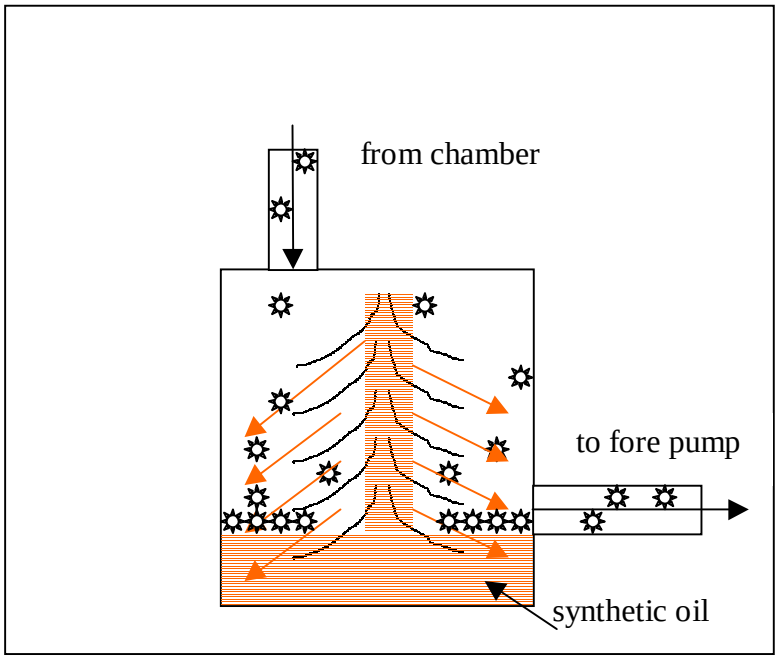

Figure 7: Diffusion Pump schematic, synthetic oil sprays from top of mechanism at center , this pumps down to $1.6x10^{-5}$ Torr

chamber and exhausts them. In the "cannon" chamber the diffusion pump is mounted directly below the chamber, which houses the oven. The cannon chamber has pumped the chamber from 1 atmosphere (760 Torr) down to $1.6x10^{-5}$ Torr in approximately thirty minutes. The schematic of the "cannon" chamber may be viewed in Figure 16. When the experimenter wishes to bring the chamber to atmosphere he must turn off both the diffusion pump and the fore pump. Then, slowly dry air may be pumped into the chamber. When the experimenter then wishes to bring the system back down to a medium vacuum level the fore pump is used by itself until the pressure is $50x10^{-2}$ Torr. Then the Diffusion pump may be turned on, however it takes quite a while for the diffusion pump oil to heat up again and become useful. This process of taking the system from a vacuum pressure to atmosphere back to a vacuum pressure can take up to thirty minutes. The other chamber has a few more safeguards and mechanisms that make its operation more convenient than the "cannon" chamber.

First, the other chamber has a trap where extra fore-pump oil, that may spill into the vacuum line between the fore pump and diffusion pump, will collect instead of clogging the vacuum line. Next, the vacuum line has three adjustable valves that can isolate the diffusion pump and the fore pump from the rest of the vacuum line. This is helpful when it becomes necessary to bring the chamber to atmosphere and then pump it back down to a medium vacuum level. In the other apparatus, both pumps may be left pumping while they are isolated from the rest of the system. All of the above may be seen in the schematic drawing of the vacuum system in Figure 8. Thus, we now understand how to create an atomic beam of Bi and isolate Bi vapor in the chamber at will. It is next necessary to examine how we populated Rydberg states.

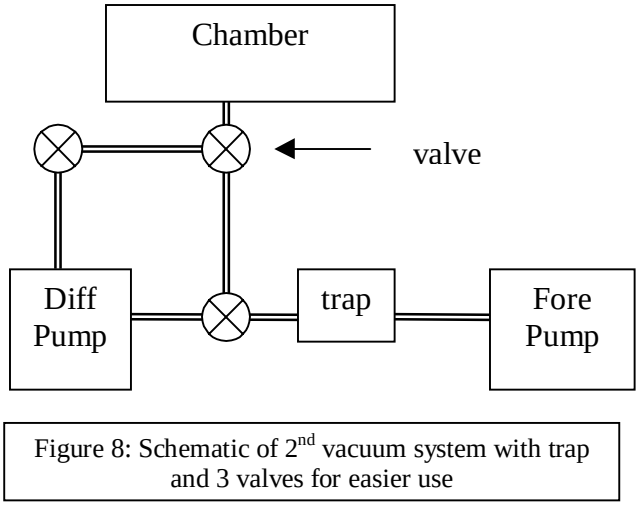

Figure 8: Schematic of 2nd vacuum system with trap and 3 valves for easier use

Laser System

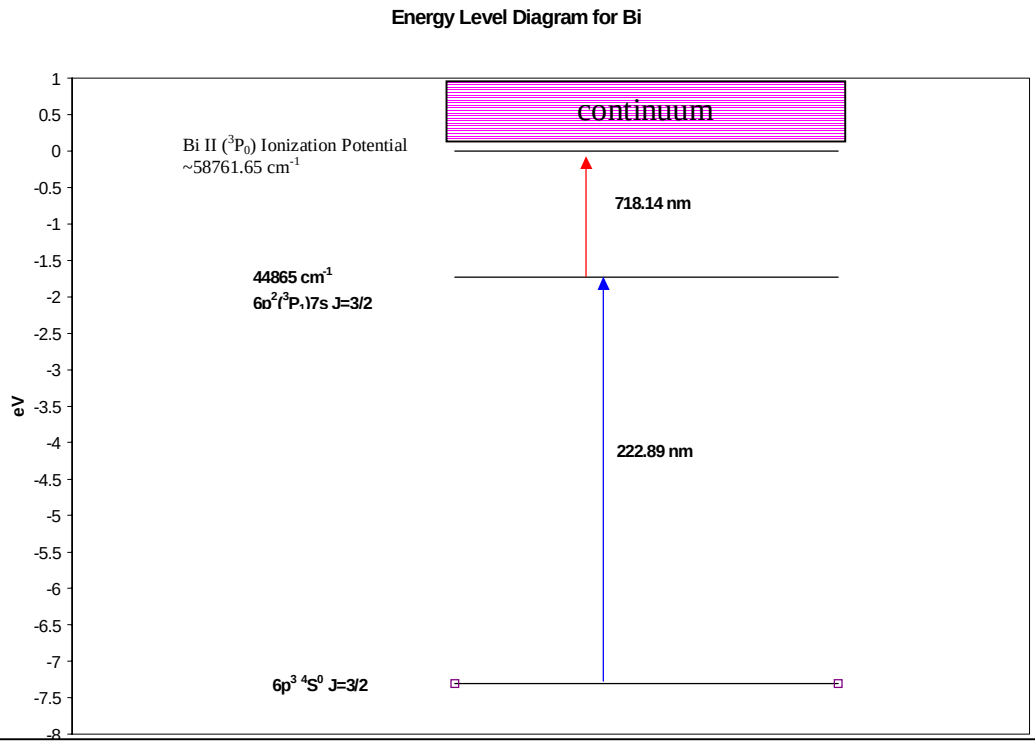

Figure 9: 1st Excitation Scheme, 445.7 nm beam is frequency doubled through a BBO crystal to give the 222.89 nm beam, electron is then excited with red beam near the IP

There were two lasers systems used in the attempt to produce photoionizing Rydberg series of Bismuth. The first system attempted to populate an odd series, the second, an even series. In this work we hoped to populate Rydberg states by using visible dye lasers. There are two different lasers simultaneously used in each of the two laser configurations. Dye lasers are relatively cheap and easy to assemble; however they are messy and require a good deal of attention. The energy level diagram shown in Figure 9 demonstrates that we wish to take one of the three p electrons in the outer shell of Bi and excite it to very near the ionization threshold using one intermediate resonance. Initially the excitation of the $6p^3\ ^4S^0_{3/2}$ to the $6p^2(^3P_1)7s$ (J=3/2) looked very promising.

This was attempted by using two Littrow laser configurations, seen in Figure 9, one with an amplifier to create a blue beam at 445.68 nm and one without the amplifier, a red beam, which was tunable to wavelengths less than 718.14 nm. This red was designed to sweep through different wavelengths to populate different states near the ionization limit. Using this construction we hoped to access states satisfying the standard selection rules and below the ionization threshold.

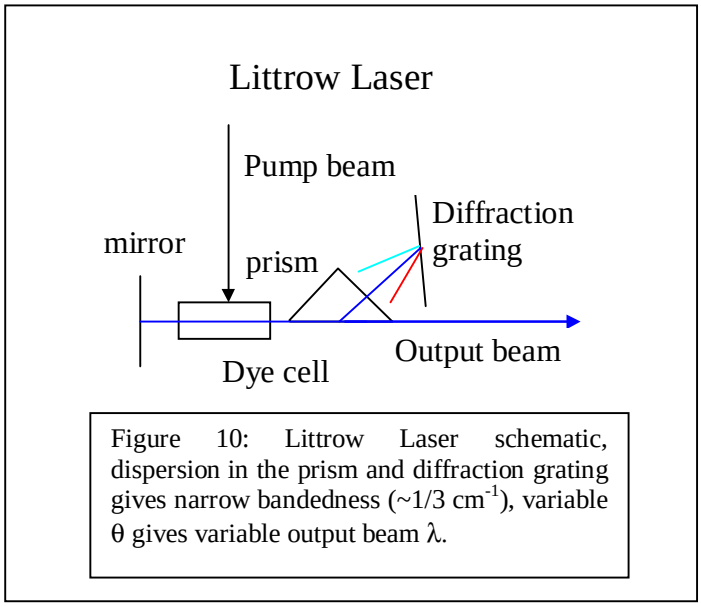

Figure 10: Littrow Laser schematic, dispersion in the prism and diffraction grating gives narrow bandedness (~1/3 cm^{-1}), variable θ gives variable output beam λ.

The Littrow laser system is constructed as follows. A pumping beam, in the case of the blue beam, with wavelength 332 nm (3^{rd} harmonic ultraviolet beam) from the Nd:YAG source, and in the case of the red laser a beam of wavelength 532 nm (2^{nd} harmonic green beam), from the Nd:YAG laser is used to excite the selected dyes. In the blue beam system, the dye used is Coumarin 440, which is dissolved in Methanol. After the pumping beam excites the dye a small signal is produced at the surface of the dye cell. This excitation causes a narrow beam sent out in all directions. Using a total reflector orthogonal to the incoming pumping beam some of the output is reflected back through the dye cell, which can amplify the initial signal. This new output is then directed toward a prism at near grazing incidence. The beam passes through a prism where blue light is bent more than red light from the normal to the surface dispersing the

different wavelengths in the beam. This outputted line is sent to the surface of a diffraction grating, which reflects light directly back if:

$$2\sin(\theta)=M\lambda/a.$$

Here θ is the angle the beam makes with the normal to the diffraction grating, M is the order of the reflected beam of the diffraction grating, λ is the wavelength in air and 1/a is the number of millimeters/line on the diffraction grating, see Figure 10. So, the diffraction grating selects a wavelength and selects it to be amplified through the dye cell again, thus completing the cavity and producing a very narrow banded laser. Bandwidths on the order of 1/3 cm^{-1} are common as can be seen in the spectrum in the following sections. The blue laser then sends this initial output through another dye cell pumped with the 3rd harmonic of the Nd:YAG laser source, further amplifying this initial output. We thus produce a 445.68 nm laser beam with a reasonable power (445 μJ). However, the separation between the ground state and the desired excited state is 44865 cm^{-1} (equivalent to 222.89 nm). This blue laser is precisely twice the wavelength necessary for the intended transition. The 445.8 nm transforms into a beam at 222.89 nm through frequency doubling.

The production of ultraviolet from blue light was not possible, however, in this instance. The BBO (β-Barium Borate) crystal used could not be phase-matched at 222.89 nm because of the angle of its cut. Not every crystal can double every conceivable wavelength of light. Since certain wavelengths of light frequency double and phase match at different angles to the normal. Holt and Cooke[21] constructed a frequency doubled 238 nm beam. This method would have worked by using a crystal, which was cut to phase match 222.89 nm, however, in the interest of economy, another

transition was selected to populate the Rydberg states of Bismuth. We searched through Atomic Energy Levels by Charlotte Moore [3] for a different transition.

The ground state, $6p^3\ {}^4S^o_{3/2}$ to $6p^2({}^3P_0)7p$ is a transition that is excitable using

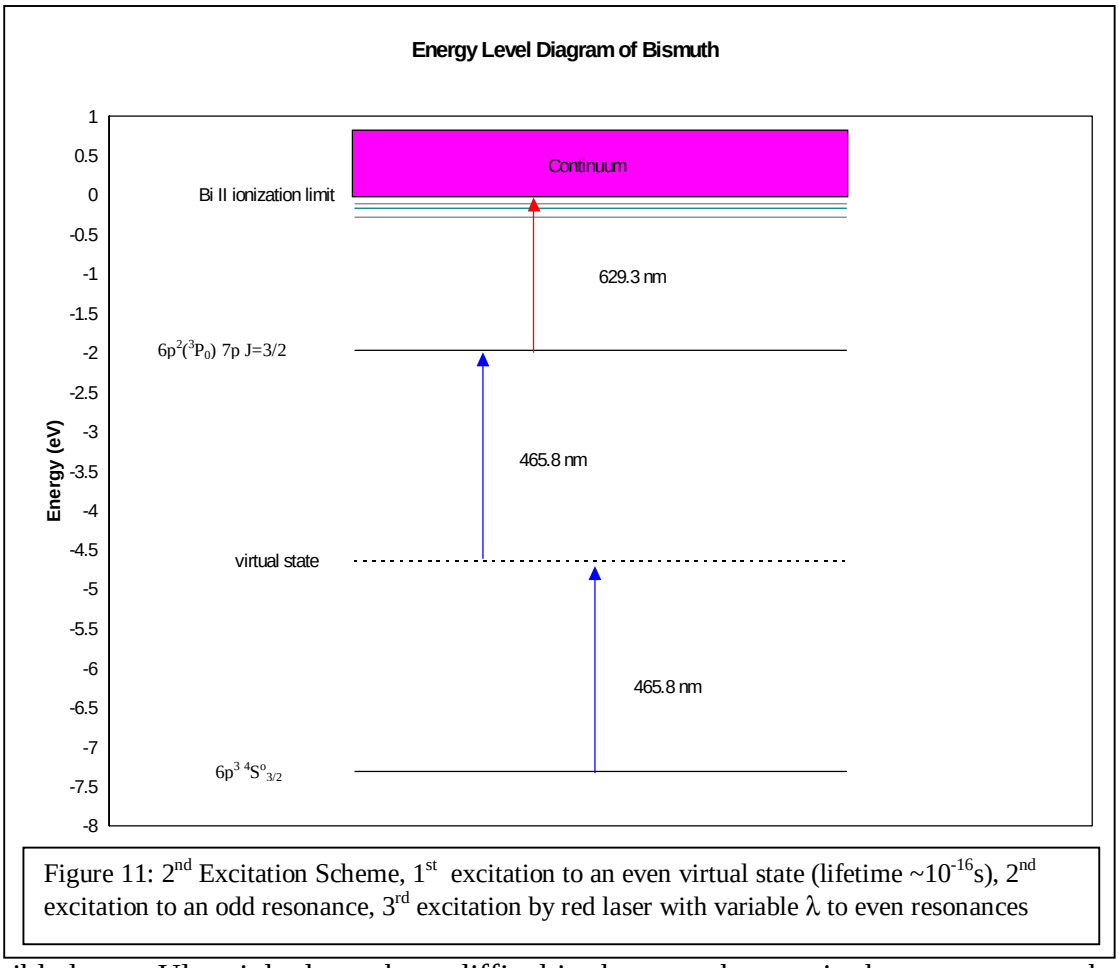

Figure 11: 2nd Excitation Scheme, 1st excitation to an even virtual state (lifetime ~10^{-16}s), 2nd excitation to an odd resonance, 3rd excitation by red laser with variable λ to even resonances

visible lasers. Ultraviolet lasers have difficulties because they are in the energy range that is necessary to dissociate air molecules, so any UV beam in air will quickly be attenuated. Therefore, visible light is preferable.

The ground state to $6p^2({}^3P_0)7p$ transition requires an energy input of 42940 cm^{-1}, laser of wavelength 232.9 nm and also a parity change[v]. This is in the ultraviolet regime, however, it is possible to drive this transition without using ultraviolet light by, instead of

[v] an even configuration to an odd, never an odd to another odd state, likewise angular momentum must change by one

using a resonant state, using a virtual state. A virtual state transition is one in which one photon is absorbed by the system, however the photon does not have the proper energy to take the system to a resonant state. These transitions due occur due to the Heisenburg Uncertainty Principle that says $\Delta E \Delta t \geq h/4\pi$. So, if two photons interact with the electrons with a small enough Δt there can be a substantial detuning. In our case we are detuned by 11119.7 cm^{-1}, which gives a necessary Δt of 2.39×10^{-16} seconds. The duration of the Quantaray pulse is on the order of nanoseconds, therefore the virtual state will be excited for 1×10^{-7} of the duration of the pulse. However, the high intensity of the beam assures that we will be able to use this virtual state. Resonant states thus have lifetimes on the order of nanoseconds, while virtual states have lifetimes many orders of magnitude

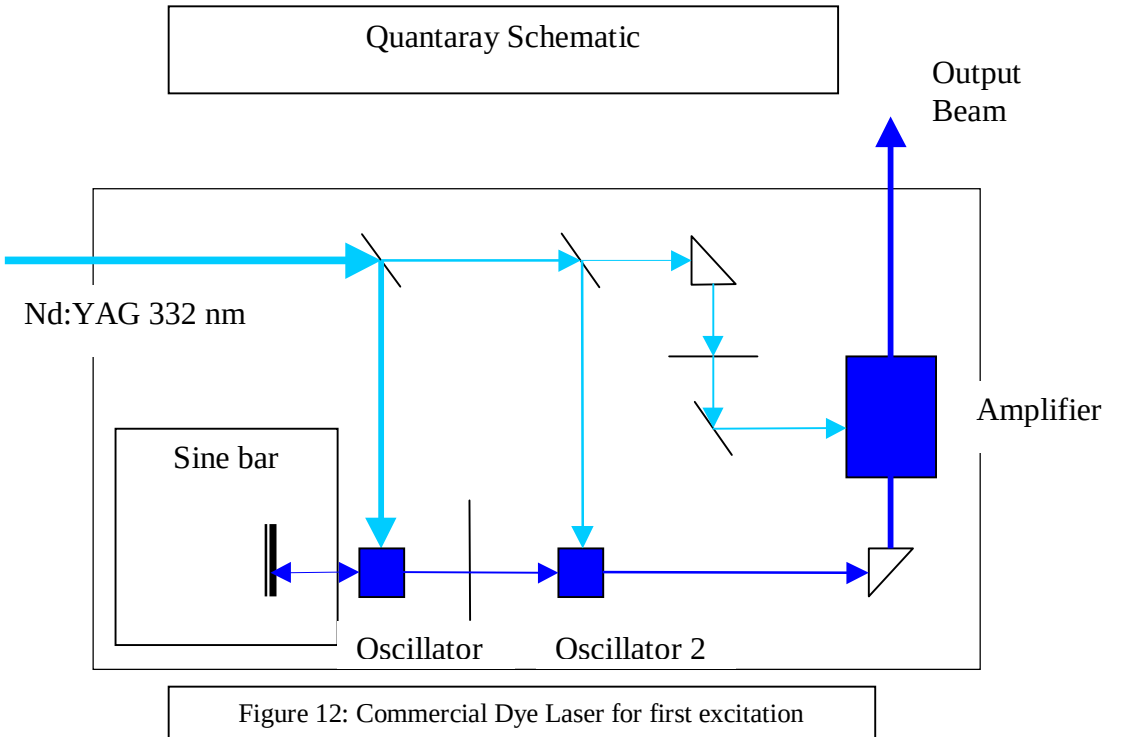

Figure 12: Commercial Dye Laser for first excitation

less than the lifetime of a resonant state[vi]. We therefore will have limited population of the 42940 cm^{-1} state, but with the high power beam we used this is not an issue. We now drive the first desired transition and have the system in the $6p^2(^3P_0)7p$ configuration by using two photons of energy 21,468.4 cm^{-1}. A commercial Quantaray laser system drives this transition. The Quantaray schematic can be seen in Figure 12. This manufactured Quantaray laser is constructed very much like the blue laser constructed for frequency doubling in the 1st system; it is a Littrow setup with amplifiers. This Quantaray laser uses two amplifiers instead of the one that we used in our blue laser. However, the outermost electron is still tightly bound, but one more visible photon will excite it to the ionization limit. Thus, we attain spectra by tuning a final visible dye laser from 630 nm to 642 nm.

There were four laser attributes that were needed for this work. First, the lasers needed to have a reasonable power[vii]. Second, the lasers needed to be narrow banded[viii]. Third, the beam needed a good spatial mode. Finally, the beam needed to be easily and continuously tunable. There were four main problems that effected the quality of this Littrow laser. First, the pump source was penetrating too far into the dye because the pumping beam was too strong. This reduced the linewidth of the resonator by allowing a wider range of angles to fall on the diffraction grating, which produces multiple wavelengths in the output beam.

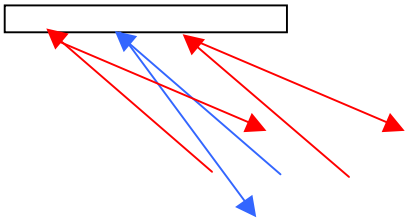

Figure 13: Poor alignment of beam, the diffraction grating selects more than one λ in a dispersed beam, grating lines are out of page

[vi] $\Delta t = \hbar/2\Delta E$

[vii] ~μJ

[viii] narrow banded = monochromatic = having a single frequency

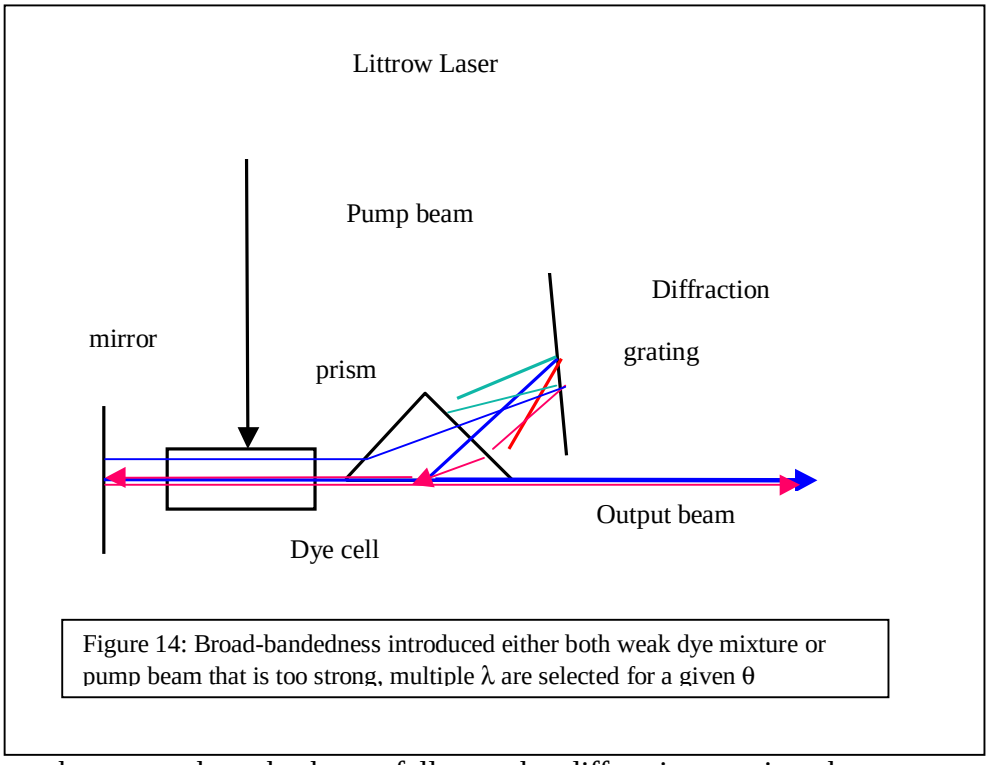

Figure 14: Broad-bandedness introduced either both weak dye mixture or pump beam that is too strong, multiple λ are selected for a given θ

This occurs because when the beam falls on the diffraction grating there are several wavelengths in the beam, which will strike the grating at different angles. So, by introducing a set of two partial reflectors the pumping beam was reduced in intensity to 4 % of the original beam intensity by each of the two partial reflectors. The second issue was that the dye was not strong enough. This results in the pumping beam penetrating too far into the dye cell just as the first concern did. These first two concerns can be seen in Figures 13 and 14. The third concern was that the beam was just not aligned well. The lines of the diffraction grating must be perpendicular to the beam path, even as the grating turns. So, the beam was aligned rigorously.

The final effect that was of concern is called Spatial Hole Burning. This occurs because there is a standing wave in the cavity between the mirror used in the Littrow apparatus and the diffraction grating. This reflected beam interferes with the initial output beam creating a superposition of the beams through the mirror-diffraction grating cavity. This standing wave gives rise to competing modes which laze at two frequencies

separated by $\Delta\nu$=1/2 cm^{-1}. This causes different frequency light to have a different number of nodes in the dye cell. This effect was minimized by adjusting the distance between the mirror and the dye cell to 2 cm. The correction of these four effects created a laser beam bandwidth successfully reduced to 1/3 cm^{-1}.

The last element of concern in the laser system is the timing of the pulses. The blue laser pulse needs to excite one of the $6p^3$ valence electrons before the red laser can excite this electron to the Rydberg state. So, the blue laser pulse must arrive before the red laser pulse. Since beams originating from the same location pump both pulses, the red beam must travel a further distance to arrive after the blue beam. Figure 14 shows the paths of the laser pulses and shows a delay of the pulses of 5 ns and an overlap for the pulses of 3 ns. The only part of the apparatus yet to be explained is the detection system, which is addressed in the following section.

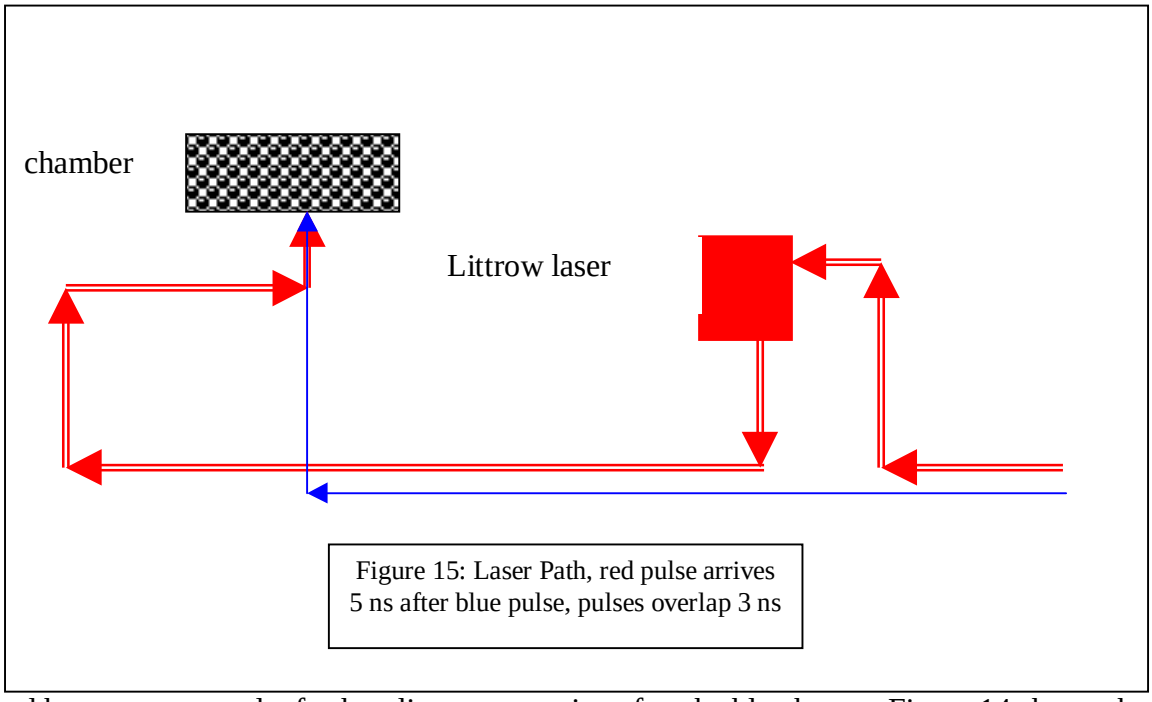

Figure 15: Laser Path, red pulse arrives 5 ns after blue pulse, pulses overlap 3 ns

Detection System

Field Ionization

As the red laser swept through different wavelengths, the Rydberg electron was excited to one of many different energy states. Low *n* states were populated using laser wavelengths, which are greater than those used to populate high *n* states. In order to detect the states in which the Rydberg electron was, a pair of screens, which can apply a pulsed potential of up to 1400 V (across 1.5 cm) to field ionize[ix] the loosely bound Rydberg electrons. This pulse is applied after the blue and red laser pulses interact with the atomic beam. In this way the potential applied will not create a Stark shift during the excitation. The purpose of applying this field is to rip loosely bound electrons from the atomic systems. The applied potential ionized the high *n* Rydberg states, while the low lying states only ionized when the Coulombic potential, which scales as $1/n^{*4}$, was less than the potential applied by the pulser.

[ix] rip loosely bound electrons from the atom

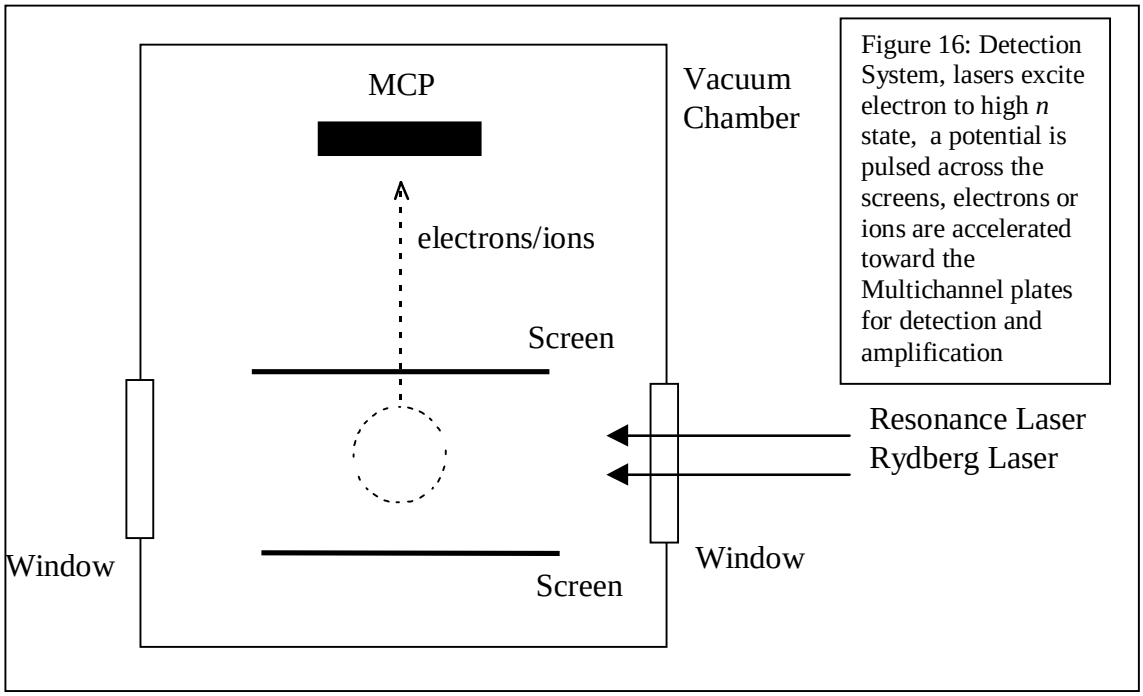

Figure 16: Detection System, lasers excite electron to high *n* state, a potential is pulsed across the screens, electrons or ions are accelerated toward the Multichannel plates for detection and amplification

Ion Detection

A voltage is applied to one of the two Multichannel plates (MCP), as can be seen in Figure 16, which then accelerates the corresponding charged particle toward the plate. To detect ions a large, 2 kV, negative voltage is applied to the front plate. When these ions hit the plate they will rapidly decelerate and, due to the nature of the material, cause a myriad of 1,000 electrons per incoming electron to be emitted from the plate. Since the front plate is carrying a large negative voltage, these electrons are accelerated away from this front plate toward a second plate, which has been grounded. This second deceleration of charged particles causes another amplification on the order of 1,000. While we have increased the amplitude of our signal many orders of magnitude it is still a very small signal by oscilloscope standards, however we can use a standard amplifier circuit to increase our amplitude by two orders of magnitude. One could also detect ions, however, there are drawbacks to detecting ions. Since ions are so massive, they do not accelerate quickly in the pulsed field. Therefore, correlation between laser wavelength

and ion signal would not be as precise as with a less massive particle, such as an electron. The other concern here was that, since the ions are so massive, the peaks in an ion spectrum are fundamentally wider than those in an electron spectrum. This is because there would be a variation in ion arrival time depending on whether the ion originated from the near or far side of the laser beam. Electrons were thus selected as the particle to be detected.

Electron Detection

The system was reconfigured by putting a high positive voltage[x] on the rear MCP, while leaving the voltage across the field ionization plates at the 1400 V previously mentioned. The system was thus configured to detect electrons. The system amplified the Rydberg electrons through two MCP amplifications as mentioned earlier. Since electrons have such a small mass to charge ration, they can be accelerated by an electric field much more quickly than ions into the Multichannel plates. This gave a fundamentally narrower peak on the oscilloscope and correlated more strictly the signal and laser wavelength. Electrons thus improved our spectrum for two reasons, first by reducing the background of charged particles and by better correlating the incident laser wavelength with the free electron concentration. Incidentally, two detection systems were used, one in the cannon system and one in the 2nd system. However, both functioned exactly the same and thus the aforementioned description applies perfectly to both. The only remaining component in this investigation is the calibration and analysis of the detected spectrum.

[x] ~2 kV

Data Analysis

Bismuth Spectrum

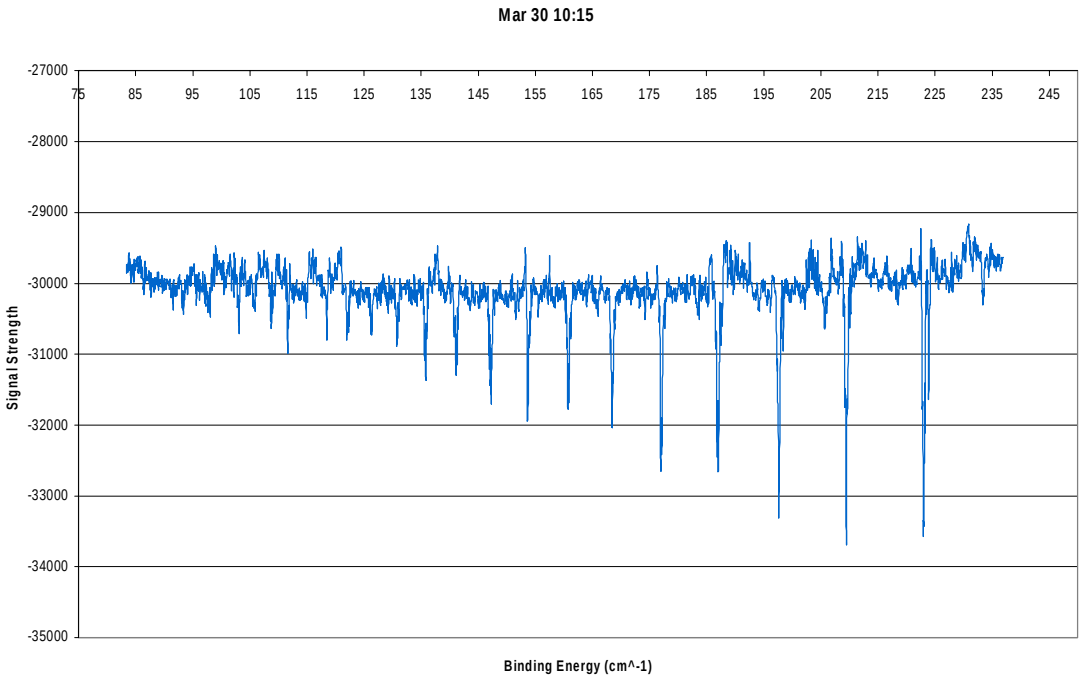

Figure 17: Bismuth Spectrum, red laser frequency was scanned giving negative peaks when the laser excited to a resonant state

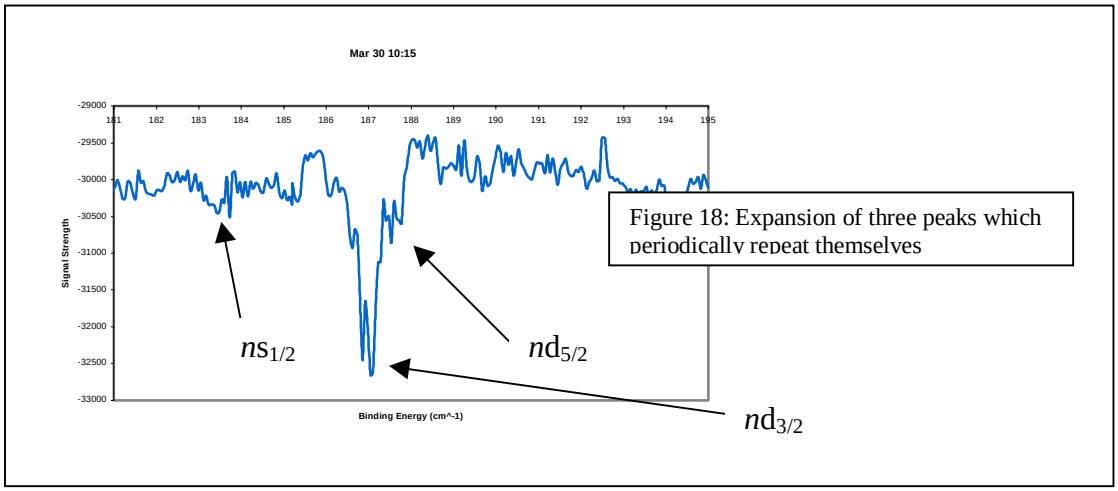

Figure 18: Expansion of three peaks which periodically repeat themselves

The data seen in Figures 17-23 was produced using the three photon excitation seen in Figure 11. The Rydberg electron begins in an odd state and since three photons are being used it can end up only in an even[xi] series. So there are three states in which the Rydberg electron may be, the $6p^2\ ns_{1/2}$, $6p^2\ nd_{3/2}$ and $6p^2\ nd_{5/2}$. These results can be

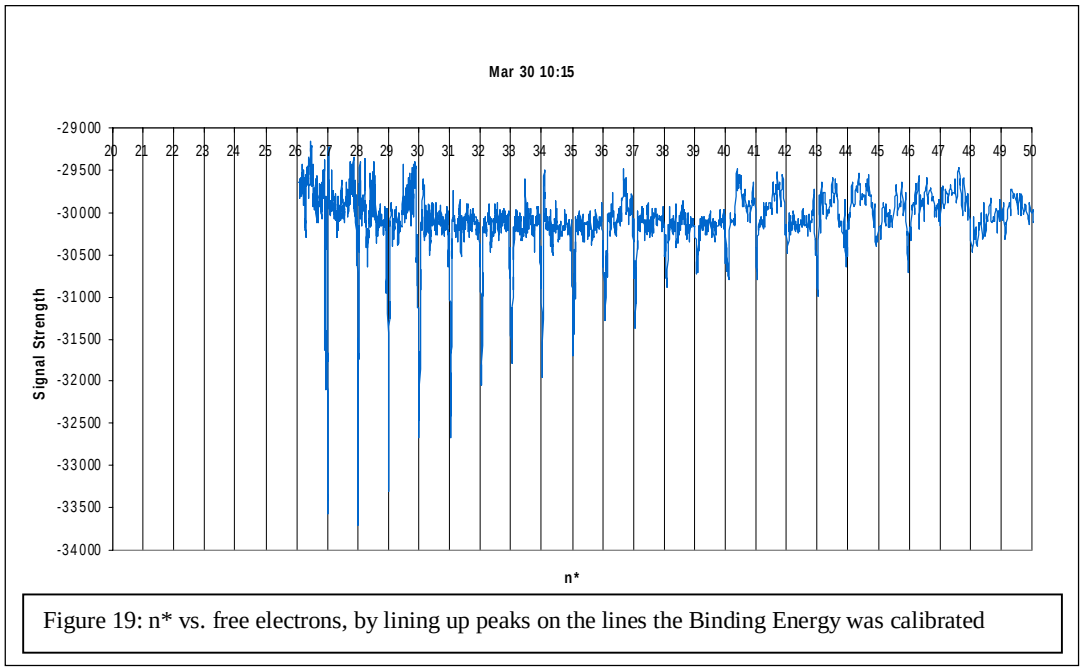

Figure 19: n* vs. free electrons, by lining up peaks on the lines the Binding Energy was calibrated

[xi] even series are states with even **L** (**L**=0,2,4,6…)

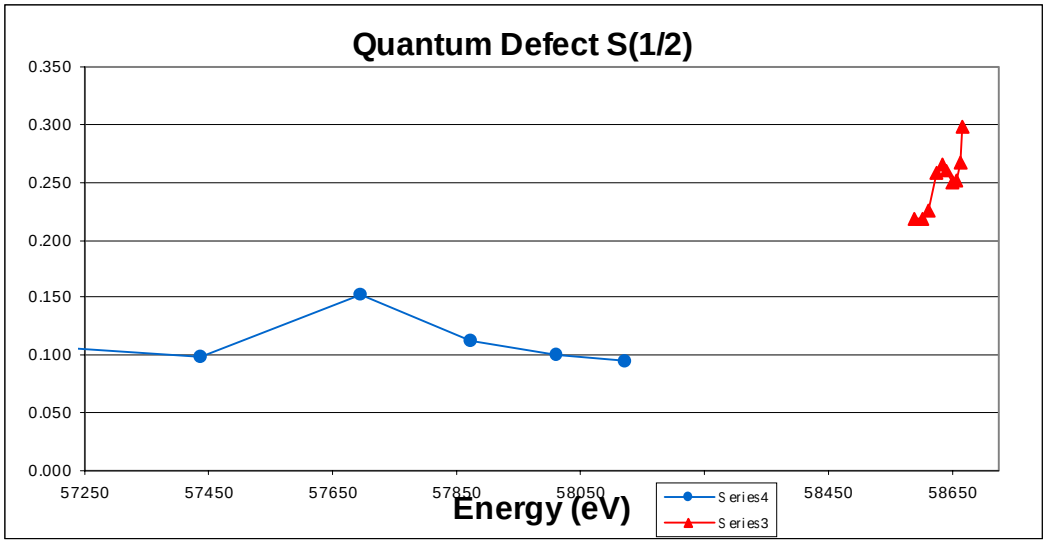

Figure 20: δ mod(1) vs. Energy for $s_{1/2}$, blue line Young, Mirza and Duley [6] with corrected data from [4], red data is newly reported data, horizontal lines imply no interaction

seen in Figure 17. Table 1 shows the signal and energies given by Young, Mirza and Duley [6], Moore [3] and Joshi and Srivastava [4][xii] with the data from this work for the $6p^2\ (^3P_0)ns_{1/2}$ and the $6p^2\ (^3P_0)nd_{5/2}$ series. While the data from the $6p^2\ (^3P_0)nd_{3/2}$ series can be seen in Table 2. The Quantum Defect plots (Figures 20-23) show that the beginning and end of the series strongly deviate from the horizontal line which was anticipated. This can be corrected only by an adjustment of the Ionization Potential which was used (58761.65 cm^{-1} [11]). Furthermore, a detailed examination of the Quantum Defect plots for the $d_{3/2,5/2}$ series ,Figure 23, shows a small sinusoidal variation. This is due to the anisotropy of the $^3P_0$ core. The relative δ changes do correspond well to those previously reported [3], [4], [6] This work thus, extends the spectrum collected previously toward higher n*'s using three photon excitation. Furthermore, this region is very interesting in the $d_{3/2}$ and $d_{5/2}$ series because there is a great deal of structure shown

[xii] previously reported energy levels are corrected 0.35 cm^{-1} to update them to the new ionization potential of 58761.65 cm^{-1} instead of the 58762 cm^{-1} determined in 1980

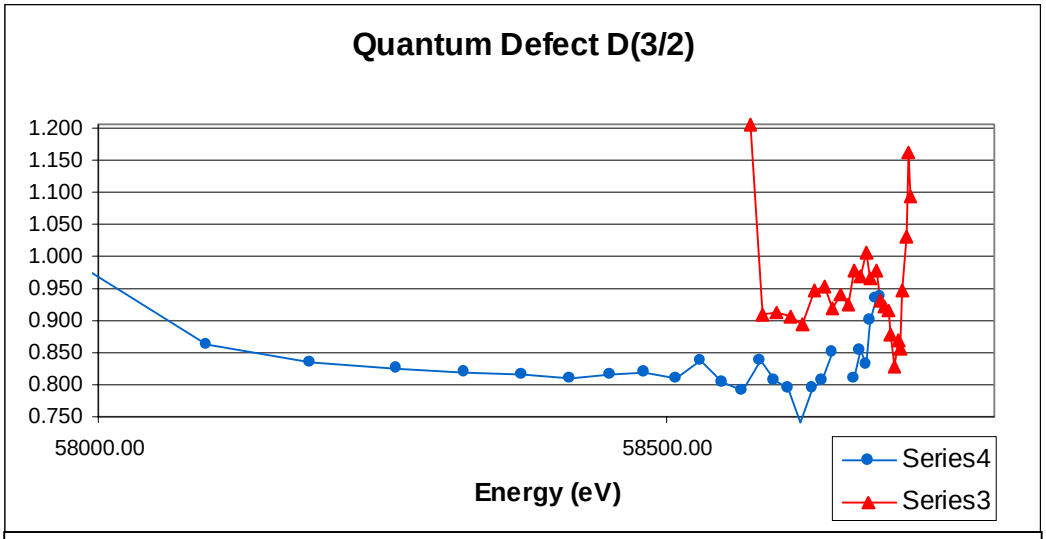

Figure 21: δ mod(1) vs. Energy for $d_{3/2}$, blue line Young, Mirza and Duley [6] with corrected data from [4], red data is newly reported data, horizontal lines imply no interaction, interaction locations between reports agree, upward slope at beginning and end of series implies different Ionization Potential, sinusoidal deviations show anisotropy of $^3P_0$ core

here. However, neither Young, Mirza and Duley [6] nor any other work has had the resolution attained in this work. Also Young, Mirza and Duley [6] were using the ionization potential of 58762 cm^{-1}, which differs from the current value of 58761.65 cm^{-1} by 0.35 cm^{-1}.

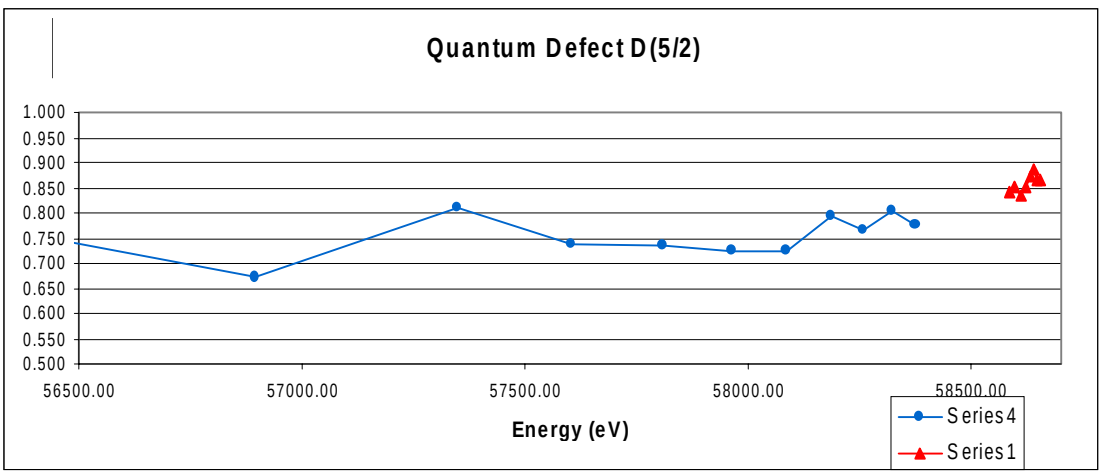

Figure 22: δ mod(1) vs. Energy for $d_{5/2}$, blue line Young, Mirza and Duley [6] with corrected data from [4], red data is newly reported data, horizontal lines imply no interaction, upward slope at beginning and end of series implies different Ionization Potential, sinusoidal deviations show anisotropy of $^3P_0$ core (magnified in Figure 23)

Table 1 (new data in bold)						
n	Source	3Po ns(1/2)	n*	Source	nd 2D(5/2)	n*
6				Joshi	44817.10	2.805
7	Moore	32588.17	2.048	Joshi	51158.00	3.799
8	Young	47373.30	3.104	Joshi	53975.00	4.788
9	Joshi	52255.00	4.107	Joshi	55474.10	5.778
10	Joshi	54557.90	5.109	Young	56360.90	6.761
11	Joshi	55823.60	6.111	Young	56896.70	7.671
12	Joshi	56590.50	7.109	Young	57347.40	8.809
13	Young	57093.50	8.111	Joshi	57604.30	9.737
14	Young	57436.10	9.099	Joshi	57809.50	10.736
15	Young	57697.00	10.153	Joshi	57963.50	11.726
16	Young	57873.10	11.113	Joshi	58084.00	12.725
17	Joshi	58012.30	12.101	Joshi	58184.80	13.793
18	Joshi	58121.80	13.096	Joshi	58258.20	14.764
19				Joshi	58322.20	15.802
20				Joshi	58371.80	16.778
21						
22						
23						
24						
25						
26						
27						
28					**58583.81**	**24.841**
29					**58597.44**	**25.851**
30		**58589.1**	**25.218**		**58609.27**	**26.836**
31		**58602.0**	**26.218**		**58620.17**	**27.850**
32		**58613.6**	**27.225**		**58630.01**	**28.872**
33		**58624.2**	**28.258**		**58638.78**	**29.885**
34		**58633.5**	**29.265**		**58646.47**	**30.867**
35		**58641.8**	**30.260**		**58653.58**	**31.866**
36		**58649.3**	**31.249**			
37		**58656.2**	**32.252**			
38		**58662.5**	**33.267**			
39		**58668.4**	**34.297**			

Table 2 (new data in bold)					
n	Source	nd 2D(3/2) Energy		n*(previous)	**n* (new)**
6	Joshi	43912.3		2.72	
7	Joshi	51018.6		3.76	
8	Joshi	53877.0		4.74	
9	Joshi	55424.7		5.73	
10	Joshi	56329.8		6.72	
11	Young	56934.6		7.75	
12	Young	57325.8		8.74	
13	Joshi	57589.7		9.68	
14	Young	57852.8		10.99	
15	Young	57981.8		11.86	
16	Young	58095.3		12.83	
17	Young	58187.5		13.82	
18	Young	58262.0		14.82	
19	Young	58322.9		15.81	
20	Young	58373.3		16.81	
21	Young	58415.9		17.82	
22	Young	58451.8		18.82	
23	Young	58482.0		19.81	
24	Young	58508.9		20.84	
25	Young	58530.8		21.80	
26	Young	58550.4		22.79	
27	Young	58568.5	**58574.33**	23.84	**24.20**
28	Young	58583.3	**58584.78**	24.81	**24.91**
29	Young	58596.7	**58598.23**	25.79	**25.91**
30	Young	58608.2	**58610.07**	26.74	**26.91**
31	Young	58619.6	**58620.60**	27.79	**27.89**
32	Young	58629.4	**58630.68**	28.81	**28.95**
33	Young	58638.5	**58639.33**	29.85	**29.95**
34	Young	58646.8	**58646.85**	30.91	**30.92**
35			**58654.08**	1.37	**31.94**
36	Young	58659.7	**58660.42**	32.81	**32.92**
37	Young	58665.9	**58666.59**	33.85	**33.98**
38	Young	58671.2	**58671.91**	34.83	**34.97**
39	Young	58676.5	**58677.00**	35.90	**36.01**
40	Young	58681.2	**58681.34**	36.93	**36.97**
41	Young	58685.4	**58685.57**	37.94	**37.98**
42	Young	58689.0	**58689.24**	38.87	**38.93**
43			**58692.79**		**39.92**
44			**58696.10**		**40.92**
45			**58699.08**		**41.88**
46			**58701.82**		**42.83**
47			**58704.63**		**43.87**
48			**58707.11**		**44.86**
49			**58709.67**		**45.95**
50			**58712.04**		**47.03**
51			**58714.34**		**48.16**
52			**58716.12**		**49.09**

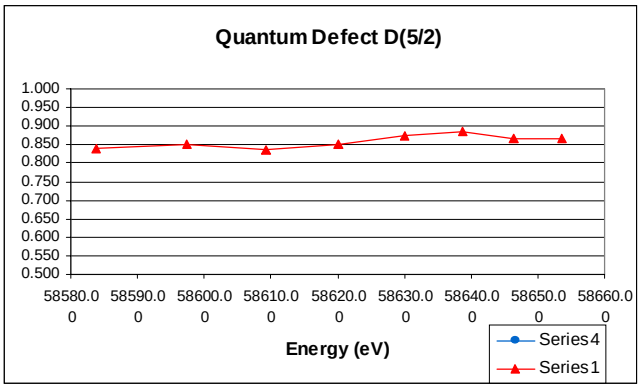

Figure 23: δ mod(1) vs. Energy for $d_{5/2,}$ sinusoidal fluctuation shows configuration interaction with anisotropic $^3P_0$ core

Laser Wavelength Calibration

As stated earlier, the diffraction equation shows how wavelength of light relates to the incident angle of the diffraction grating. However, because the Littrow laser system, which was used in this work, has both a prism for diffracting the laser beam and the diffraction grating the simplistic diffraction equation cannot give energies to the precision needed to identify quantum defects in Bismuth. By simultaneously recording an etalon pattern, with a constant peak spacing of 2.06 cm^{-1}, we were able to calibrate a motor step scale into an energy scale seen in Figure 17.

An étalon is a system of two pieces of glass with reflective coating on them. This reflective coating will transmit some wavelengths and reflect others. This series of reflective pieces of glass create a resonant cavity, which will cause an interference pattern, which depends on the frequency of the incident beam. Furthermore, since

$$f = c/\lambda=(N+\varepsilon)FSR,$$

where FSR is the free spectral range ε is a small phase shift and N is an integer, the free spectral range for the given etalon is 2.06 cm^{-1}. A plot of the pattern given by an etalon output incident on a photodiode, can be seen in Figure 24. This signal shows that the

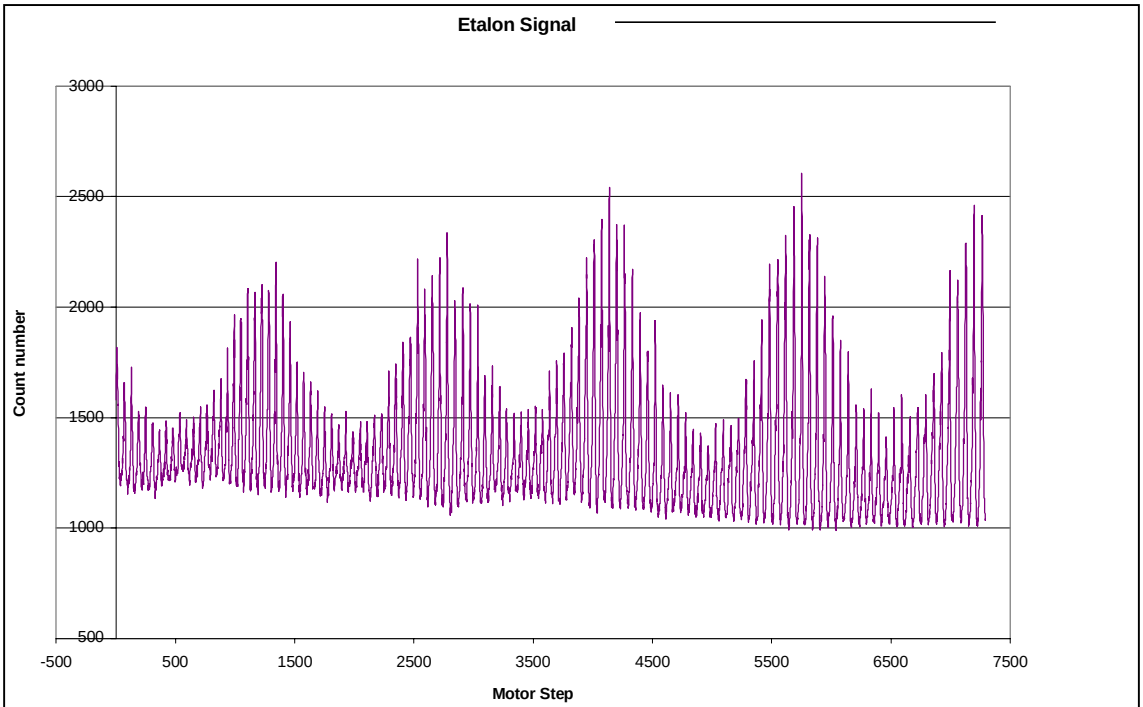

Figure 24: Étalon signal, peaks are evenly spaced in energy (2.06 cm^{-1}), signal gives relative calibration of laser wavelength and energy of resonant states

étalon signal has peaks that are not linear in motor step. Being able to predict the positions of the etalon peaks allows one to map motor step into binding energy[xiii].

[xiii] Energy necessary to ionize the system

Conclusion

Through inspection of Tables 1 and 2 and Figures 17-23 this work lines up very well with the previous work in the regions where there is overlap. Therefore, in the regions where this is the first data recorded, we expect this data to be extremely accurate. Furthermore the n* plot shows that the $6p^2\ (^3P_0)\ ns_{1/2}$ state is also perturbed as in the previous work, however the large slope at the beginning and end of this data implies that the current Ionization Potential of 58761.65 cm^{-1} needs to be revised. This work also shows that the $6p^2\ (^3P_0)\ nd_{3/2}$ is perturbed in higher *n* than was originally reported. Finally, this work gives a much better resolved view of the highly structured $6p^2\ (^3P_0)\ nd_{3/2}$, $6p^2\ (^3P_0)\ nd_{5/2}$ perturber interactions including anisotropic interactions. Further data will be taken using a system of two etalons and a HeNe laser. This system will allow for an absolute calibration of the energy scale in Figure 17 by using the interference pattern of the well known 632.8 nm HeNe laser beam.

Acknowledgements

I would just like to express my sincerest thanks for everyone who helped me to complete this work. Special thanks to Wei Yang, for helping with everything from cleaning the diff pump to firing up the CPM laser to test for Bismuth, to Kathy-Anne Brickman who gave incredible moral and intellectual support throughout my whole four years. Thanks especially to Dr. Cooke, for the unselfish way he gives his time and talent to his students always.

[1] P. Zeeman, E. Back, and S. Goudsmit, *Zeits. f. Physik*, **66**, 1
[2] Mrozowski S, *Phys. Rev.*, **62**, 526
[3] Moore C E, Atomic Energy Levels Volume III, US Govt Printing Office, Washington, DC, 1971, pp 219-23, (Original publication: *Atomic Energy Levels* NBS Circular no 467, vol 3 (Washington, DC:Us Govt Office) pp. 208-10, 219-20
[4] Joshi Y N and Srivastava R P, 1978, *Can. J. Phys.*, **56**, 1157-64
[5] N. A. Kuebler and L. S. Nelson, *J. Chem. Phys.*, **37**, 47
[6] Young, Mirza, Duley, *J. Phys. B: At. Mol. Phys*, 1980
[7] George S, Munsee J H and Vergés J, *J. Opt. Soc. Am.* **B 2**, 1264
[8] J. Connes, *et al.*, *Nouv. Rev. Opt. Appl.*, **1**, 3
[9] Buhler B, Cremer C and Gerber G, *Z. Phys. A*, **320**, 71
[10] Mazzoni, M, Joshi Y N, Nencioni A, Grisendi T and Parkinson W H, *J. Phys. B: At. Mol. Phys.*, **20**, 2193
[11] Mathews C W, Ginter M L, Ginter D S and Brown C M, *J. Opt. Soc. Am.*, **B 6** 1627
[12] C. M. Brown, R. H. Naber, S. G. Tilford, and M. L. Ginter, *Appl. Opt.*, **12** (1973), 1858
[13] R K Yoo, B Ruscic and J Berkowitz, *J. Phys. B: At. Mol. Opt. Phys.*, **28** (1995), 1743
[14] EP Buurman, OJ Koning, A. Donszelmann, *J. Phys. B: Atom. Molec. Phys.* **22**(1989), 3965
[15] W. E. Cooke, T. F. Gallagher, S. A. Edelstein, and R. M. Hill, *Phys. Rev. Letters*, **40** (1978), 178
[16] Dajun Ding, Mingxing Jin, Hang Liu and Xuewen Liu, *J. Phys. B: Atom. Molec. Phys.* **22** (1989), 1979
[17] J. Dembczynski, E. Stachowska, M. Wilson, P. Buch, W. Ertmer, *Phys Rev. A* **49** (1994) 745
[18] Handbook for Chemistry and Physics 54th edition, Chemical Ruber Company Publishing Company, Cleveland, Ohio, 1973
[19] N Bowering et al, *J. Phys. B: At. Mol. Opt. Phys*, **31** 5221
[20] Brickman, Precision Measurements of the Autoionizing States of Strontium in an Electric Field, May 2001, College of William & Mary
[21] A. Holt, W. E. Cooke, Doubled Frequency Dye Laser, August 2000, College of William & Mary